Chemical Science

EDGE ARTICLE

Check for updates

Controllable synthesis of perovskite solid solutions as novel energetic materials *via* thermodynamic equilibrium

Min Li,[a] Dandan Han, (ID) *[a] Zheng Lin,[b] Xiujuan Qi,[c] Honglei Xia,*[b] Zhao Wang, (ID) [a] Qinghua Zhang (ID) *[b] and Junbo Gong (ID) [a]

Perovskite solid solutions have aroused interest in energy applications, owing to the capability of fine-tuning and enhancing performance to surpass ternary perovskites. Their synthesis, however, is hard to control in solution due to the intricate self-assembly process wherein components crystallize in undetermined ratios. Herein, we present a facile approach to the controllable synthesis of perovskite solid solutions in aqueous solution and develop perovskite solid solutions as a novel class of energetic materials for the first time. Specifically, the composition control of perovskite solid solutions is achieved through thermodynamic equilibrium of reaction crystallization in water, exhibiting a linear relationship with the natural logarithm of reactant concentrations. Based on Goldschmidt's rule, we design a general formula of energetic perovskite solid solutions as $(H_2dabco)(NH_4)_{(1-x)}M_x(ClO_4)_3$, in which $0 < x < 1$, H_2dabco^{2+} refers to 1,4-diazabicyclo[2.2.2]octane-1,4-diium, and M is a quaternary ion. The as-synthesized $(H_2dabco)(NH_4)_{(1-x)}(Na)_x(ClO_4)_3$ exhibits exceptional thermal stability, outperforming its ternary perovskite prototypes, and the prepared $(H_2dabco)(NH_4)_{(1-x)}Ag_x(ClO_4)_3$ manifests energy-safety optimization as elevated energy levels with improved mechanical sensitivity. This work not only exploits perovskite solid solutions as a novel class of energetic materials with promising properties but also provides a means for controllably synthesizing perovskite solid solutions for versatile advanced applications.

Introduction

Seeking new strategies for designing energetic materials (EMs) with remarkable properties is a long-term pursuit.[1–4] While conventional organic synthesis of energetic molecules with oxidizing functional groups often entails experimental hazards and complex synthesis routes,[5–8] molecular perovskite energetic crystals (MPECs) integrating determined oxidizers and reductive fuels into a perovskite structure of ABX₃ have emerged as a promising alternative for EMs, owing to their high performance, low cost, and controllable experimental risks.[9–12] MEPCs are typically organic–inorganic hybrid perovskites, consisting of an organic amine cation at the A site, a small cation such as Na⁺ or NH₄⁺ at the B site, and an oxidizing anion, for example, ClO_4^-, at the X site. One reported MEPC $(H_2dabco)(NH_4)(ClO_4)_3$ known as DAP-4 (H_2dabco^{2+} refers to 1,4-diazabicyclo[2.2.2]

octane-1,4-diium), for instance, exhibits noteworthy comprehensive performance with a high decomposition temperature and good overall detonation performance rivaling cyclotrimethylene trinitramine (RDX, a renowned energetic compound).[13]
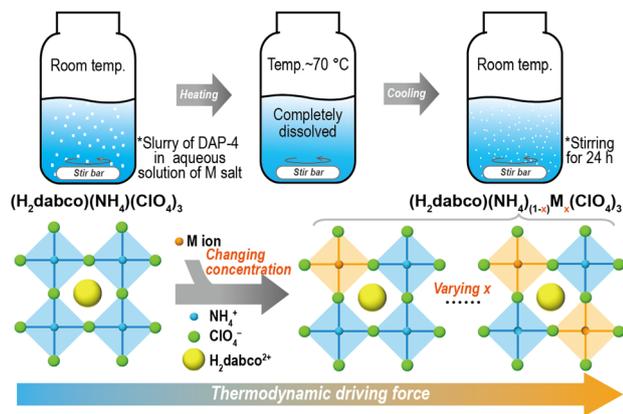
Perovskite solid solutions, composed of multiple cations or anions with variable stoichiometric ratios in isostructural perovskite structures,[14–16] are capable of fine-tuning material properties such as phase transitions,[17,18] mechanical properties,[19] and thermal stability,[20] showing great potential in outperforming ternary MPECs. However, they had not been developed for the application of EMs, owing to the nascent stage of MPECs and the paucity of appropriate synthesis methods. Conventional preparation of perovskite solid solutions includes solution-based methods,[21] vapor deposition,[22] and solid-state reactions.[23–25] Since the processing requiring high temperatures or mechanical stimuli should be minimized for EMs, mild solution-based methods can serve as a potentially viable approach for preparing energetic perovskite solid solutions (EPSSs). However, the composition of solid solutions is hard to control since the self-assembly of solid solutions in aqueous solution is an intricate process involving thermodynamics and kinetics, during which multiple ions react with each other and form a crystalline solid with components in undetermined ratios.[21,26]

[a]*State Key Laboratory of Chemical Engineering, School of Chemical Engineering and Technology, Tianjin University, Tianjin 300072, People's Republic of China. E-mail: handandan@tju.edu.cn*

[b]*National Key Laboratory of Solid Propulsion, School of Astronautics, Northwestern Polytechnical University, Xi'an 710072, People's Republic of China. E-mail: xia_honglei@nwpu.edu.cn; qinghuazhang@nwpu.edu.cn*

[c]*School of Chemistry and Chemical Engineering, Northwestern Polytechnical University, Xi'an 710129, People's Republic of China*

Scheme 1 Schematic diagram of synthesizing $(H_2dabco)(NH_4)_{(1-x)}$-$M_x(ClO_4)_3$ perovskite solid solutions through reaction crystallization in water.

Herein, we report a facile route to synthesize EPSSs with controllable compositions *via* thermodynamic equilibrium during reaction crystallization in water (Scheme 1). Goldschmidt's rule is applied to design the formula of EPSSs with thermodynamic preference. The Goldschmidt tolerance factor t is a reliable index to predict a stable perovskite structure, defined as $t = (r_A + r_X)/\sqrt{2}(r_B + r_X)$, where r_A, r_B, and r_X represent the radius of ions at the A, B, and X sites, respectively.[27] It is generally thought that cubic perovskites can be formed in the range of $0.8 < t < 1$, and t is equal to 1 for ideal stable cubic perovskites.[28] Thus, the designed EEPSs with a general formula of $(H_2dabco)(NH_4)_{(1-x)}M_x(ClO_4)_3$ ($0 < x < 1$), in which the M ion as a quaternary component makes the tolerance factor closer to 1 compared to DAP-4 ($t = 0.964$), can be synthesized by reaction crystallization of DAP-4 driven by thermodynamics.

Specifically, as shown in Scheme 1, first, DAP-4 was put into an aqueous solution of the water-soluble salt of M ions, in which the M salt was completely dissolved while DAP-4 remained incompletely dissolved at room temperature. Under heat, a homogenous aqueous solution with free organic and inorganic ions was obtained. Then, it was naturally cooled to room temperature and stirred for 24 h. The system reached its thermodynamic equilibrium and led to a stable composition in the crystalline product, achieving the controllable synthesis of EPSSs in aqueous solution.

Experimental

Materials

Sodium chloride (NaCl, MACKLIN), silver perchloride (AgClO_4, MACKLIN), and 1,4-diazabicyclo[2.2.2]octane (MACKLIN) were purchased in AR grade from MACKLIN, and 70% perchloric acid was from GHTECH. Ammonium perchlorate (AP) was self-prepared by the reaction of ammonium bicarbonate with perchloric acid. DAP-4 and DAP-1 were prepared following the reported method,[9] and the samples were slurried in water for 24 h to refine the particles and improve the crystallinity.

Synthesis of $(H_2dabco)(NH_4)_{(1-x)}Na_x(ClO_4)_3$ solid solutions

Na^+ was exemplified as the M ion in $(H_2dabco)(NH_4)_{(1-x)}M_x(ClO_4)_3$. First, 300 mg of DAP-4 and a certain weight of NaCl were added to 5 mL of deionized water. Under heat, the slurry was completely dissolved at around 70 °C. Then, the homogeneous aqueous solution was cooled naturally with a stirring speed of 150 rpm, accompanied by the crystallization of $(H_2$-dabco$)(NH_4)_{(1-x)}Na_x(ClO_4)_3$. The crystalline samples underwent filtration after stirring for 24 h. Different compositions (the value of x) were obtained by changing the initial concentration of NaCl.

Synthesis of $(H_2dabco)(NH_4)_{(1-x)}Ag_x(ClO_4)_3$ solid solutions

Moreover, the M ion in $(H_2dabco)(NH_4)_{(1-x)}M_x(ClO_4)_3$ can be an Ag^+ ion. Similarly, replacing NaCl with AgClO_4, $(H_2$-dabco$)(NH_4)_{(1-x)}Ag_x(ClO_4)_3$ solid solutions were synthesized. Different compositions (the value of x) were obtained by changing the initial concentration of AgClO_4.

Characterization

The powder X-ray diffraction (PXRD) patterns were recorded on an X-ray diffractometry system (Bruker D8 Advance, Germany) operated at 40 mA and 40 kV using Cu-Kα radiation ($\lambda = 1.5418$ Å). The metal content of the samples was measured by inductively coupled plasma mass spectrometry (ICP-MS, Agilent-5110) with the pretreatment of microwave digestion. The morphology and the elemental analysis of the solid solutions were observed using a scanning electron microscopy-energy dispersive spectrometer (SEM-EDS, GeminiSEM 360, Zeiss). Single-crystal X-ray diffraction (SCXRD) was performed on a Rigaku XtaLAB Synergy-S X-ray diffractometer using Mo Kα radiation ($\lambda = 0.71073$ Å). Differential scanning calorimeter (DSC) curves were recorded on a Mettler Toledo instrument from 35 °C to 500 °C at a set heating rate, under an atmosphere of Ar at 50 mL min^{-1}. The measurements of friction sensitivity and impact sensitivity were carried out using a standard BAM Fallhammer and a BAM friction tester, respectively.

Results and discussion

At first, given that balancing the cubic perovskite with a material that has a large tolerance factor can further stabilize its structure[29] and the tolerance factor of $(H_2dabco)(Na)(ClO_4)_3$ (DAP-1, $t = 1.029$) is larger than that of DAP-4 ($t = 0.964$), $(H_2$-dabco$)(NH_4)_{(1-x)}Na_x(ClO_4)_3$ solid solutions were designed. By fixing the feed of DAP-4 and changing the initial concentration of NaCl, a series of $(H_2dabco)(NH_4)_{(1-x)}Na_x(ClO_4)_3$ samples were obtained in pure single-phase perovskite structures without impure phases, remaining isostructural to DAP-4 in a cubic crystal system, confirmed by PXRD as shown in Fig. 1a. Note that both DAP-4 and DAP-1 here were self-prepared powder particles with good crystallinity. For the $(H_2dabco)(NH_4)_{(1-x)}$-$Na_x(ClO_4)_3$ samples, the main peak of the (400) plane shifted from 24.57° to 24.91° compared to DAP-4, indicating the contraction of the d-spacing, while the peak for DAP-1 appeared at 25.21°, with a small d-spacing. The Na element is distributed
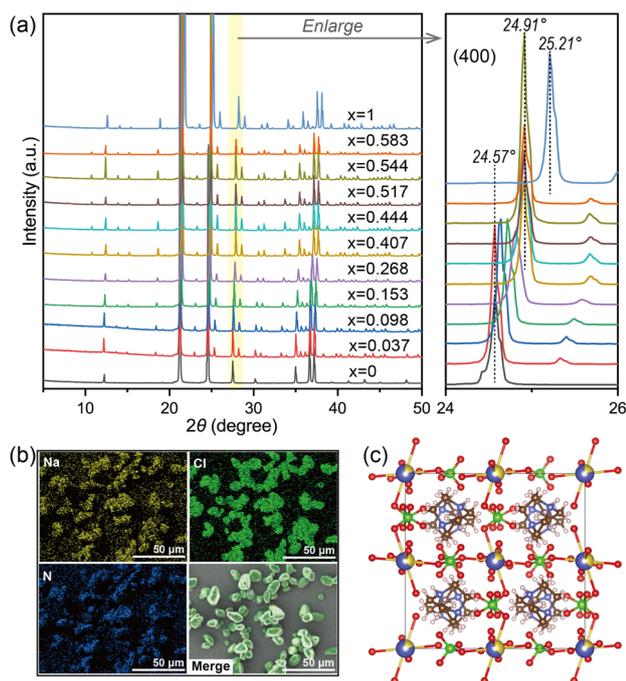
Fig. 1 (a) PXRD patterns of $(H_2dabco)(NH_4)_{(1-x)}Na_x(ClO_4)_3$ samples (x = 0 for DAP-4, and x = 1 for DAP-1). (b) SEM-EDS elemental maps of Na, Cl, and N, and the merged map for $(H_2dabco)(NH_4)_{0.483}(Na)_{0.517}(ClO_4)_3$. (c) The crystal structure of $(H_2dabco)(NH_4)_{0.715}Na_{0.285}(ClO_4)_3$, with Na in yellow, N in blue, Cl in green, O in red, and C in brown, and the hydrogens of the ammonium are omitted.

uniformly in the crystalline particles (Fig. 1b), as demonstrated by SEM-EDS. Validated by the single-phase PXRD patterns and the uniform distribution of Na, the $(H_2dabco)(NH_4)_{(1-x)}Na_x(ClO_4)_3$ solid solutions were successfully synthesized. The content of Na element in the solid solutions was quantified by ICP-MS. Based on the measured Na content, we calculated the value of x in $(H_2dabco)(NH_4)_{(1-x)}Na_x(ClO_4)_3$.

To verify the crystal structure of the solid solutions, we synthesized single crystals through cooling crystallization, using the powder sample prepared with an equal ratio of DAP-4 and Na^+ in water as the raw material. Then, the single-crystal structure of $(H_2dabco)(NH_4)_{0.715}Na_{0.285}(ClO_4)_3$ was obtained by

SCXRD as listed in Table S1. As anticipated, the structure of $(H_2dabco)(NH_4)_{0.715}Na_{0.285}(ClO_4)_3$ is in a cubic crystal system with the space group of $Pa\bar{3}$, isostructural to DAP-4; and the Na^+ and the NH_4^+ ions occupy the same positions in the crystal structure (Fig. 1c). In addition, the content of Na in the single-crystal structure (1.52 wt%) is approximately consistent with that of the powder sample (1.43 wt% obtained by ICP-MS).

During the crystallization, the formation of $(H_2dabco)(NH_4)_{(1-x)}Na_x(ClO_4)_3$ can be considered as a series of reactions with variable stoichiometry as follows ($0 < x < 1$).

$$(H_2dabco)NH_4(ClO_4)_3 + xNaCl \rightarrow$$
$$(H_2dabco)(NH_4)_{(1-x)}Na_x(ClO_4)_3 + xNH_4Cl \quad (1)$$
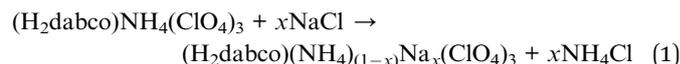
Indeed, the value of x not only indicates the composition of the perovskite solid solution but also represents the extent of reaction, reflecting changes in the concentrations of reactants and products. As shown in Fig. 2a, the molar ratio of Na^+ and NH_4^+ ions in the final crystalline particles was inconsistent with the feeding ratio; in contrast, the value of x is linearly proportional to the natural logarithm of the initial concentration of Na^+ (Fig. 2b). The driving force of both reaction and crystallization is the difference in the chemical potentials of reactants and products, and the chemical potential of the compound is linearly correlated with the natural logarithm of its concentration in solution according to thermodynamics. In this case, the initial concentration of NaCl directly manipulates the chemical potentials of reactants, modulates the thermodynamic driving force of reaction crystallization, and affects the reaction route, leading to varying stoichiometry. At last, the whole system reaches the thermodynamic equilibrium of both reaction and crystallization, where the Gibbs free energy of the system reaches a minimum, determining the crystalline composition of solid solutions. When the concentration of NaCl in water was the largest (about 6.34 mol L^{-1} for saturated NaCl at ambient temperature), x reached 0.583, indicating that the composition of $(H_2dabco)(NH_4)_{(1-x)}Na_x(ClO_4)_3$ solid solutions is thermodynamically preferred in the range of $0 < x \leq 0.583$.

Accordingly, the effective tolerance factor (t_{eff}) was calculated using the average radius at the B site for $(H_2dabco)(NH_4)_{(1-x)}Na_x(ClO_4)_3$ solid solutions, applying the following equations:[29]
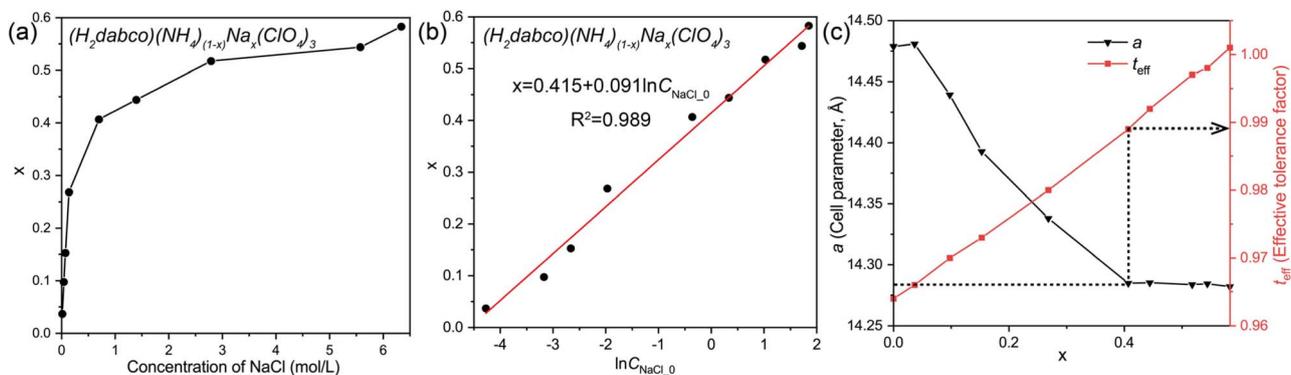

Fig. 2 (a) Changes in x with the concentration of NaCl. (b) The curve of x correlating with the logarithm of the initial concentration of NaCl in aqueous solution. (c) The calculated cell parameter a and the effective tolerance factor t_{eff} for each $(H_2dabco)(NH_4)_{(1-x)}(Na)_x(ClO_4)_3$.

$$\overline{r_B} = (1-x)r_1 + xr_2 \qquad (2)$$

$$t_{\text{eff}} = \frac{r_A + r_X}{\sqrt{2}\left[r_X + \overline{r_B}\right]} \qquad (3)$$

where r_1 and r_2, in this case, represent the radii of NH_4^+ and Na^+, respectively. As shown in Fig. 2c, the calculated t_{eff} for each sample is higher than the t of DAP-4 (0.964) and increases to around 1, following Goldschmidt's rule for ideal cubic perovskites. Moreover, the cell parameter a for each sample was calculated based on PXRD data (the detailed data for $(H_2dabco)(NH_4)_{(1-x)}Na_x(ClO_4)_3$ solid solutions and the prepared DAP-1 and DAP-4 are listed in Tables S2 and S3). The cell parameter a is linearly related to x in a certain range (Fig. 2c), owing to the characteristic of solid solutions that the unit-cell dimensions remain isostructural and change gradually with stoichiometry.[30,31] Then, the cell parameter remains around 14.285 Å for $0.407 \leq x \leq 0.583$ with a value of t_{eff} between 0.989 and 1.001, which may be due to the constraint from the geometric dimension of the components and the interactions in the crystal structure.

As the solid solutions need to be thermodynamically preferred compared to DAP-4 to induce a thermodynamic driving force for reaction crystallization and Goldschmidt's rule can semi-empirically predict the thermodynamic stability of the cubic perovskite structure,[28] we generalized a formula of EPSSs, i.e., $(H_2dabco)(NH_4)_{(1-x)}M_x(ClO_4)_3$, where the M^+ ion should have a smaller ion radius compared with NH_4^+ (1.67 Å),[32] decreasing the average radius at the B site and making the value of t_{eff} reach 1 (Fig. 3). Moreover, $(H_2dabco)(NH_4)_{(1-x)}M_x(ClO_4)_3$ should have a value of t_{eff} closer to 1 compared to both DAP-4 and $(H_2dabco)M(ClO_4)_3$, ensuring its thermodynamic preference to enable reaction crystallization.

Given the radius of the Ag^+ ion of 1.28 Å, another demonstration of EPSSs, $(H_2dabco)(NH_4)_{(1-x)}Ag_x(ClO_4)_3$ solid solutions, was synthesized through similar reaction crystallization using water-soluble silver perchlorate ($AgClO_4$) as the silver source (the information about the samples is detailed in Table S4). The Ag element was distributed uniformly in the crystalline particles (Fig. 4a), and the cubic perovskite structure was retained from DAP-4 (Fig. 4b and S1), demonstrating the
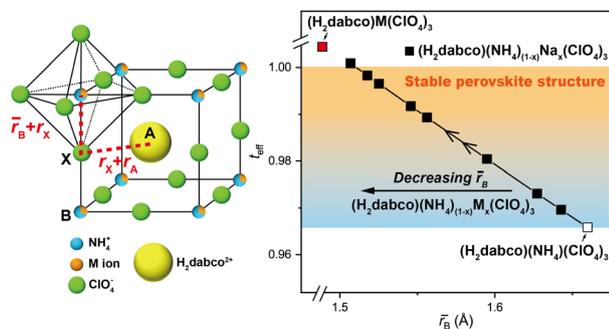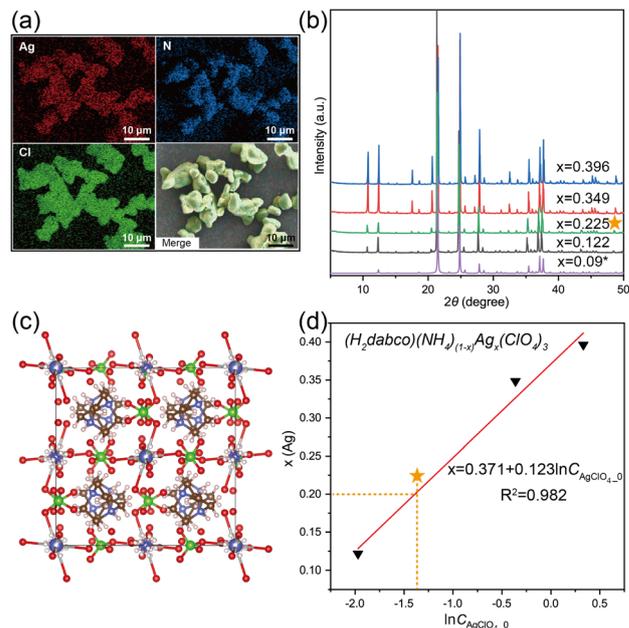

Fig. 4 (a) SEM–EDS elemental maps of Ag, Cl, and N, and the merged map for $(H_2dabco)(NH_4)_{0.651}Ag_{0.349}(ClO_4)_3$. (b) PXRD patterns of $(H_2dabco)(NH_4)_{(1-x)}Ag_x(ClO_4)_3$ (the asterisk for the simulated PXRD). (c) The crystal structure of $(H_2dabco)(NH_4)_{0.91}Ag_{0.09}(ClO_4)_3$, with Ag in gray, N in blue, Cl in green, O in red, and C in brown. (d) The fitting curve of x in $(H_2dabco)(NH_4)_{(1-x)}Ag_x(ClO_4)_3$ correlating with the natural logarithm of initial concentrations of $AgClO_4$. The triangle symbols in (d) refer to the experimental samples, and the stars in (b and d) indicate the product obtained under the designated initial concentration.

successful synthesis of solid solutions. One single-crystal structure, $(H_2dabco)(NH_4)_{0.91}Ag_{0.09}(ClO_4)_3$, was obtained by SCXRD (Table S5), with Ag^+ and NH_4^+ ions sharing the same B sites (Fig. 4c). Also, the composition of $(H_2dabco)(NH_4)_{(1-x)}Ag_x(ClO_4)_3$ is controlled by the initial concentrations of $AgClO_4$, yielding a linear fitting curve of x as a function of the natural logarithm of the initial concentration ($R^2 = 0.982$) based on three solid solution samples (Fig. 4d). The curve is supposed to guide the synthesis of the $(H_2dabco)(NH_4)_{(1-x)}Ag_x(ClO_4)_3$ with a target composition. For example, when the initial concentration of $AgClO_4$ was designated as 0.249 mol L^{-1} according to the fitting curve aiming for $x = 0.2$, the product was identified as $(H_2dabco)(NH_4)_{0.775}Ag_{0.225}(ClO_4)_3$ by ICP-MS with a content of Ag that was close to the anticipated value (Fig. 4d).

Furthermore, the EPSSs exhibit intriguing properties compared to ternary MPECs (partly listed in Table 1, and the concerning properties of all involved samples are detailed in Table S7). For the $(H_2dabco)(NH_4)_{(1-x)}Na_x(ClO_4)_3$ solid solutions ($0 < x \leq 0.583$), the thermal decomposition temperature increases by up to 12 °C with rising x and exceeds those of both DAP-1 and DAP-4, surpassing most of the reported MPECs (Fig. S2).

Specifically, as listed in Table 1, $(H_2dabco)(NH_4)_{0.715}Na_{0.268}(ClO_4)_3$ slightly elevates the peak temperature of decomposition by about 6.5 °C in comparison to DAP-4; and the increase in the peak temperature for $(H_2dabco)(NH_4)_{0.483}Na_{0.517}(ClO_4)_3$ reaches 13 °C compared to DAP-4 and 8 °C

Fig. 3 The simplified structure of the cubic perovskite solid solution (left) and the illustration of stable $(H_2dabco)(NH_4)_{(1-x)}M_x(ClO_4)_3$ solid solutions as the $\overline{r_B}$ decreases and the t_{eff} increases (right).

Table 1 Comparison of the properties of the perovskite solid solutions and the involved ternary perovskites

Samples	Density[b] [g cm^{-3}]	T_{onset}[c] [°C]	T_p[c] [°C]	Friction sensitivity[d] [N]	Impact sensitivity[d] [J]
(H$_2$dabco)(NH$_4$)(ClO$_4$)$_3$ [DAP-4]	1.88	360.07	386.64	36	>40
(H$_2$dabco)Na(ClO$_4$)$_3$ [DAP-1]	2.05	373.28	391.70	48	>40
(H$_2$dabco)(NH$_4$)$_{0.732}$Na$_{0.268}$(ClO$_4$)$_3$	1.95	371.72	393.14	40	>40
(H$_2$dabco)(NH$_4$)$_{0.483}$Na$_{0.517}$(ClO$_4$)$_3$	1.97	377.98	399.95	48	>40
(H$_2$dabco)(NH$_4$)$_{0.878}$Ag$_{0.122}$(ClO$_4$)$_3$	2.02	347.20	383.82	14	>40
(H$_2$dabco)(NH$_4$)$_{0.651}$Ag$_{0.349}$(ClO$_4$)$_3$	2.14	309.45	380.27	12	>40
(H$_2$dabco)Ag(ClO$_4$)$_3$ [DAP-5][a]	2.42[a]	313.2[a]	313.6[a]	≤5[a]	3[a]

[a] The data of DAP-5 were from ref. 38, while other data were from this work. [b] The density was calculated based on PXRD data. [c] T_{onset} and T_p are the onset temperature and peak temperature obtained at 10 K min^{-1} for the samples besides DAP-5. [d] The measurements of friction sensitivity and impact sensitivity were performed on a BAM friction tester and a standard BAM Fallhammer, respectively.

relative to DAP-1, with similar increases observed in the onset temperature. Performing thermal analysis,[33,34] the apparent activation energy of the two solid solutions is lower than that of either DAP-1 or DAP-4, indicating the fast energy release during thermal decomposition (DSC curves at varied heating rates are shown in Fig. S3 and the calculated results are listed in Table S6). On the other hand, the free energy of activation ($G^{\neq}$) calculated for (H$_2$dabco)(NH$_4$)$_{0.483}$Na$_{0.517}$(ClO$_4$)$_3$ surpassed that of both DAP-1 and DAP-4 (Table S6), signifying its high energy barrier for thermal decomposition, resulting in exceptional thermal stability.[35]

As for (H$_2$dabco)(NH$_4$)$_{(1-x)}$Ag$_x$(ClO$_4$)$_3$ solid solutions, the thermal behavior can outperform that of the ternary (H$_2$dabco)Ag(ClO$_4$)$_3$ (DAP-5) as shown in Table 1 and Fig. S4. Notably, the (H$_2$dabco)(NH$_4$)$_{(1-x)}$Ag$_x$(ClO$_4$)$_3$ solid solutions can boost the energy density compared to DAP-4 while with available processing safety as friction sensitivity between 12 and 20 N and impact sensitivity exceeding 40 J, in comparison to DAP-5, which is highly sensitive to mechanical stimulus with poor processability.[36] Moreover, (H$_2$dabco)(NH$_4$)$_{(1-x)}$Na$_x$(ClO$_4$)$_3$ solid solutions had values of friction sensitivity between 32 and 48 N, approaching that of DAP-1 (48 N) and mostly higher than that of DAP-4 (36 N), less sensitive to the friction stimulus compared with DAP-4. In addition, all the prepared powder samples were insensitive to impact stimulus with a value of impact sensitivity of over 40 J, which may result from the effect of fine particles and good crystallinity with few defects.[37,38]

Also, the detonation performance of EPSSs was preliminarily evaluated through the measurements of constant-volume combustion energy and the Kamlet–Jacobs (K–J) equation.[39,40] The calculation of detonation parameters, including detonation heat, velocity, and pressure, is detailed in the SI with the corresponding data listed in Tables S8–S12. Remarkably, the detonation parameters of (C$_6$H$_{14}$N$_2$)(NH$_4$)$_{0.732}$Na$_{0.268}$(ClO$_4$)$_3$ surpass those of both DAP-4 and DAP-1. (C$_6$H$_{14}$N$_2$)(NH$_4$)$_{0.732}$Na$_{0.268}$(ClO$_4$)$_3$ only contains a small amount of Na (1.43 wt%) and generates a similar content of gaseous products to DAP-4 during detonation, while its density, enthalpy of formation, and the average molar mass of gaseous products (due to the reduction of HCl and N$_2$ gaseous products) are higher than those of DAP-4 in Table S11. Therefore, its overall detonation performance is superior to that of DAP-4 according to the K–J equation. Besides, the overall detonation performance of

(C$_6$H$_{14}$N$_2$)(NH$_4$)$_{0.483}$Na$_{0.517}$(ClO$_4$)$_3$ is inferior to that of DAP-4 (Table S11). It may be due to its high content of Na, resulting in lower generation of gaseous products compared to DAP-4. As for (H$_2$dabco)(NH$_4$)$_{0.878}$Ag$_{0.122}$(ClO$_4$)$_3$ and (H$_2$dabco)(NH$_4$)$_{0.651}$Ag$_{0.349}$(ClO$_4$)$_3$ solid solutions, though their detonation heat and detonation velocity are not comparable to those of DAP-4, they exhibit excellent detonation pressure, which may result from their high density due to the incorporation of Ag. It can be concluded that EPSSs in certain compositions, for example, with a small amount of Na or Ag, which have a high density without significantly decreasing gaseous products, can potentially exhibit high detonation performance and surpass ternary MPECs.

Conclusions

In summary, we develop perovskite solid solutions as novel EMs, providing a novel platform for designing advanced EMs. Energetic (H$_2$dabco)(NH$_4$)$_{(1-x)}$M$_x$(ClO$_4$)$_3$ solid solutions in cubic perovskite structures are designed based on Goldschmidt's rule and synthesized through reaction crystallization in water. The composition control can be achieved through thermodynamic equilibrium, exhibiting a linear relationship with the natural logarithm of the initial concentration of M salt. The proposed methodology enables the composition control of molecular perovskite solid solutions in aqueous solution. Moreover, the as-synthesized EPSSs demonstrate remarkable performance, as the thermal stability of (H$_2$dabco)(NH$_4$)$_{(1-x)}$(Na)$_x$(ClO$_4$)$_3$ outperforms that of its ternary perovskite prototypes, and (H$_2$dabco)(NH$_4$)$_{(1-x)}$Ag$_x$(ClO$_4$)$_3$ manifests energy-safety optimization with elevated energy levels and improved mechanical sensitivity. Furthermore, EPSSs in certain compositions with high density and generating comparable gaseous products can possess enhanced detonation performance, surpassing ternary MPECs. It is demonstrated that fine-tuning the composition of EPSSs can endow EMs with superior properties, including thermal stability, energy-safety optimization, and detonation performance. This work not only provides a feasible approach for preparing perovskite solid solutions as promising EMs but also enlightens the role of thermodynamic equilibrium in the synthetic methodology of perovskite solid solutions, promoting the rational design of perovskite solid solutions for versatile applications.

Author contributions

M. Li: investigation, methodology, conceptualization, and writing – original draft. H. Dan: funding acquisition and writing – review & editing. Z. Lin: investigation. X. Qi: investigation and resources. H. Xia: investigation, funding acquisition, and writing – review & editing. Z. Wang: resources. Q. Zhang: resources, writing – review & editing, supervision, and funding acquisition. J. Gong: supervision.

Conflicts of interest

There are no conflicts to declare.

Data availability

CCDC 2465024 and 2465025 contain the supplementary crystallographic data for this paper.[41a,b]

The data supporting this article have been included in the main text and the supplementary information (SI). Supplementary information: Tables S1–S12, Fig. S1–S4, thermal analysis, and detonation performance. See DOI: https://doi.org/10.1039/d5sc05641a.

Acknowledgements

References

1 M. K. Bellas and A. J. Matzger, *Angew. Chem., Int. Ed. Engl.*, 2019, **58**, 17185–17188.

2 H. M. Titi, J. M. Marrett, G. Dayaker, M. Arhangelskis, C. Mottillo, A. J. Morris, G. P. Rachiero, T. Friščić and R. D. Rogers, *Sci. Adv.*, 2019, **5**, eaav9044.

3 Y. Wang, Y. Liu, S. Song, Z. Yang, X. Qi, K. Wang, Y. Liu, Q. Zhang and Y. Tian, *Nat. Commun.*, 2018, **9**, 2444.

4 W. Qian, A. Mardyukov and P. R. Schreiner, *Nature*, 2025, **642**, 356–360.

5 A. T. Nielsen, A. P. Chafin, S. L. Christian, D. W. Moore, M. P. Nadler, R. A. Nissan, D. J. Vanderah, R. D. Gilardi, C. F. George and J. L. Flippen-Anderson, *Tetrahedron*, 1998, **54**, 11793–11812.

6 P. F. Pagoria, G. S. Lee, A. R. Mitchell and R. D. Schmidt, *Thermochim. Acta*, 2002, **384**, 187–204.

7 J. Ma, A. K. Chinnam, G. Cheng, H. Yang, J. Zhang and J. M. Shreeve, *Angew. Chem., Int. Ed. Engl.*, 2021, **60**, 5497–5504.

8 J. Singh, R. J. Staples and J. M. Shreeve, *Sci. Adv.*, 2023, **9**, eadk3754.

9 S.-L. Chen, Z.-R. Yang, B.-J. Wang, Y. Shang, L.-Y. Sun, C.-T. He, H.-L. Zhou, W.-X. Zhang and X.-M. Chen, *Sci. China Mater.*, 2018, **61**, 1123–1128.

10 Y. Feng, J. Zhang, W. Cao, J. Zhang and J. M. Shreeve, *Nat. Commun.*, 2023, **14**, 7765.

11 S. Chen, Y. Gao, C. Dong, L. Shen, Y. Zeng, P. Bao, Y. Li, Z. Yi, H. Chen, S. Zhu and L. Zhang, *Adv. Sci.*, 2025, **12**, 2415680.

12 C.-X. Yu, L. Ye, H. Zhuo, Y.-F. Yan and W.-X. Zhang, *Inorg. Chem. Front.*, 2025, **12**, 4645–4652.

13 W.-X. Zhang, S.-L. Chen, Y. Shang, Z.-H. Yu and X.-M. Chen, *Energ. Mater. Front.*, 2020, **1**, 123–135.

14 L. He, P.-P. Shi, M.-M. Zhao, C.-M. Liu, W. Zhang and Q. Ye, *Chem. Mater.*, 2021, **33**, 799–805.

15 W.-Q. Liao, D. Zhao, Y.-Y. Tang, Y. Zhang, P.-F. Li, P.-P. Shi, X.-G. Chen, Y.-M. You and R.-G. Xiong, *Science*, 2019, **363**, 1206–1210.

16 D. Shin, M. Lai, Y. Shin, J. S. Du, L. Jibril, J. M. Rondinelli and C. A. Mirkin, *Adv. Mater.*, 2023, **35**, e2205923.

17 T. H. Chan, N. T. Taylor, S. Sundaram and S. P. Hepplestone, *J. Phys. Chem. C*, 2022, **126**, 13640–13648.

18 A. Ray, B. Martín-García, A. Moliterni, N. Casati, K. M. Boopathi, D. Spirito, L. Goldoni, M. Prato, C. Giacobbe, C. Giannini, F. Di Stasio, R. Krahne, L. Manna and A. L. Abdelhady, *Adv. Mater.*, 2022, **34**, 2106160.

19 M. K. Mishra, U. Ramamurty and G. R. Desiraju, *J. Am. Chem. Soc.*, 2015, **137**, 1794–1797.

20 D. Vujovic, H. Raubenheimer and L. Nassimbeni, *Eur. J. Inorg. Chem.*, 2004, **2004**, 2943–2949.

21 A. Mancini, P. Quadrelli, C. Milanese, M. Patrini, G. Guizzetti and L. Malavasi, *Inorg. Chem.*, 2015, **54**, 8893–8895.

22 X. Song, Q. Cui, Y. Liu, Z. Xu, H. Cohen, C. Ma, Y. Fan, Y. Zhang, H. Ye, Z. Peng, R. Li, Y. Chen, J. Wang, H. Sun, Z. Yang, Z. Liu, Z. Yang, W. Huang, G. Hodes, S. Liu and K. Zhao, *Adv. Mater.*, 2020, **32**, 2003353.

23 T. Wang, J. Fan, C. L. Do-Thanh, X. Suo, Z. Yang, H. Chen, Y. Yuan, H. Lyu, S. Yang and S. Dai, *Angew. Chem., Int. Ed. Engl.*, 2021, **60**, 9953–9958.

24 J. Moriguchi, T. Koga, N. Tsunoji, S. Nishihara, T. Akutagawa, A. Masuya-Suzuki and R. Tsunashima, *Chem. Commun.*, 2024, **60**, 12181–12184.

25 S. Jiang, T. Hu, J. Gild, N. Zhou, J. Nie, M. Qin, T. Harrington, K. Vecchio and J. Luo, *Scr. Mater.*, 2018, **142**, 116–120.

26 J. Peng, C. Q. Xia, Y. Xu, R. Li, L. Cui, J. K. Clegg, L. M. Herz, M. B. Johnston and Q. Lin, *Nat. Commun.*, 2021, **12**, 1531.

27 V. M. Goldschmidt, *Naturwissenschaften*, 1926, **14**, 477–485.

28 Q. Sun and W.-J. Yin, *J. Am. Chem. Soc.*, 2017, **139**, 14905–14908.

29 Z. Li, M. Yang, J.-S. Park, S.-H. Wei, J. J. Berry and K. Zhu, *Chem. Mater.*, 2015, **28**, 284–292.

30 M. Lusi, *Cryst. Growth Des.*, 2018, **18**, 3704–3712.

31 W. Cao, X. Yang, C. Genevois, M. Allix and X. Kuang, *Inorg. Chem.*, 2021, **60**, 3282–3290.

32 V. Sidey, *Acta Crystallogr.*, 2016, **72**, 626–633.

33 H. E. Kissinger, *Anal. Chem.*, 1957, **29**, 1702–1706.

34 H. Ma, B. Yan, Z. Li, Y. Guan, J. Song, K. Xu and R. Hu, *J. Hazard. Mater.*, 2009, **169**, 1068–1073.

35 E. An, S. Chen, X. Li, Y. Tan, X. Cao and P. Deng, *Can. J. Chem.*, 2021, **100**, 328–337.

36 Y. Shang, S.-L. Chen, Z.-H. Yu, R.-K. Huang, C.-T. He, Z.-M. Ye, W.-X. Zhang and X.-M. Chen, *Inorg. Chem.*, 2022, **61**, 4143–4149.

37 M. Li, X. Zhou, J. Wang, Q. Zhang, D. Han, J. Gong and H. Li, *Small*, 2025, **21**, 2500829.

38 H. Li, X. Zhou, R. Xu, S. Hao, D. Chen and X. Zhou, *Energ. Mater. Front.*, 2020, **1**, 178–185.

39 M. J. Kamlet and S. J. Jacobs, *J. Chem. Phys.*, 1968, **48**, 23–35.

40 Y. Wang, J. Zhang, H. Su, S. Li, S. Zhang and S. Pang, *J. Phys. Chem. A*, 2014, **118**, 4575–4581.

41 (*a*) CCDC 2465024: Experimental Crystal Structure Determination, 2025, DOI: **10.5517/ccdc.csd.cc2nr1xd**; (*b*) CCDC 2465025: Experimental Crystal Structure Determination, 2025, DOI: **10.5517/ccdc.csd.cc2nr1yf**.